XI International Conference on Computational Plasticity. Fundamentals and Applications
COMPLAS XI
E. Oñate, D.R.J. Owen, D. Peric and B. Suárez (Eds)

HYDRO-MECHANICAL MODELING OF TWO-PHASE FLUID FLOW IN DEFORMING, PARTIALLY SATURATED POROUS MEDIA WITH PROPAGATING COHESIVE CRACKS USING THE EXTENDED FINITE ELEMENT METHOD

TOKTAM MOHAMMADNEJAD[*] AND AMIR REZA KHOEI[†]

[*]Center of Excellence in Structural and Earthquake Engineering, Department of Civil Engineering
Sharif University of Technology
P.O. Box. 11365-9313, Tehran, Iran
email: toktammd@yahoo.com

[†] Center of Excellence in Structural and Earthquake Engineering, Department of Civil Engineering
Sharif University of Technology
P.O. Box. 11365-9313, Tehran, Iran
email: arkhoei@sharif.edu

Key words: Deformable, fracturing and partially saturated porous medium, Two-phase fluid flow, Cohesive crack propagation, Extended finite element method (XFEM), Fully coupled model.

Abstract. In the present paper, a fully coupled numerical model is developed for the hydro-mechanical analysis of deforming, progressively fracturing porous media interacting with the flow of two immiscible, compressible wetting and non-wetting pore fluids. The governing equations involving the coupled two-phase fluid flow and deformation processes in partially saturated porous media containing cohesive cracks are derived within the framework of the generalized Biot theory. The displacement of the solid phase, the pressure of the wetting phase and the capillary pressure are taken as the primary unknowns of the three-phase formulation. A softening cohesive law is employed to describe the nonlinear behavior of the material in the fracture process zone. In order to account for the flux of the two fluid phases through the fracture faces, the mass balance equation for each flowing fluid inside the fully damaged zone and the cohesive zone is averaged over its cross section. The resulting equations provide mass couplings to the standard equations of the multiphase system. The effect of cracking and therefore change of porosity on the permeability of the damaged zone is also taken into account. To arrive at the discrete equations, the extended finite element method (XFEM) is utilized to discretize the weak form of the balance equations of mass and linear momentum in spatial domain along with the Generalized Newmark scheme for time domain discretization. By exploiting the partition of unity property of finite element shape functions, the evolving cohesive crack is simulated independently of the underlying finite element mesh and without continuous remeshing of the domain as the crack grows by adding enriched degrees of freedom to nodes whose support is bisected by the crack. For the numerical solution, the unconditionally stable direct time-stepping procedure is applied to solve the resulting system of strongly coupled non-linear algebraic equations using a Newton-Raphson iterative procedure. Finally, numerical simulations are presented to demonstrate the capability of the proposed method and the significant influence of the hydro-mechanical coupling between the continuum porous medium and the discontinuity on the results.

1 INTRODUCTION

The present paper focuses on the hydro-mechanical modeling of two-phase fluid flow in deforming, partially saturated porous media containing propagating cohesive cracks, which has practical applications in a broad range of engineering areas. In the literature, the topic of fluid flow in fractured/fracturing porous media has been dealt with in different ways: in [1] a numerical procedure for the simulation of hydraulically-driven fracture propagation in poroelastic materials has been presented combining the finite element method with the finite difference method, in [2] the problem of hydraulic cohesive crack growth in fully saturated porous media has been solved using the finite element method with mesh adaptation, in [3] a hydro-mechanical formulation for fully saturated geomaterials with pre-existing discontinuities has been presented based on the finite element method with zero-thickness interface elements, and the subject of fluid flow in fractured fully saturated systems and in fracturing unsaturated systems with passive gas phase has been treated in [4] and [5], respectively, using the extended finite element method, which is now extended to three-phase porous media. The three-phase numerical model developed here is based upon the mechanics of deformable porous media on the basis of the generalization of the Biot theory in conjunction with the cohesive fracture mechanics, which provides a suitable framework to describe the coupled hydro-mechanical and fracture mechanisms occurring in fracturing, multiphase porous media. In such multiphase systems, the coupling between the flow of the wetting and non-wetting phases in the pore spaces of the continuous porous medium and the discontinuity, the deformation of the solid phase, the fluid exchange between the discontinuity and the surrounding porous medium and the possible development of the discontinuity across which the cohesive tractions are transmitted is usually strong, which demands the fully coupled treatment of the problem. In the formulation presented herein, all these components are brought together to thoroughly simulate the deforming, partially saturated porous medium behavior in the presence of geomechanical discontinuities, thus exhibiting fluid flow, deformation and fracture processes properly.

The extended finite element method combined with the cohesive crack model yields an efficient approach to simulate the cohesive crack propagation [6-8]. In fracturing, partially saturated porous media, the crack growth occurs as the progressive decay of the cohesive tractions transferred across the fracture process zone and the imposition of the mean pore pressure onto the crack faces by means of the pore fluids within the crack. The tractions acting on the fracture faces give rise to the mechanical coupling between the fracture and the medium surrounding the fracture. Besides, the flux of the two fluid phases through the fracture borders leads to the mass transfer coupling, which is a subject of great interest in hydraulic fracturing.

2 THE PHYSICAL MODEL

The pores of the solid skeleton in the partially saturated porous medium are assumed to be filled up partly with water (w) and partly with gas (g). Thus, degrees of saturation of the liquid phase S_w and the gaseous phase S_g always sum to unity, i.e. $S_w + S_g = 1$. The capillary pressure between the two fluid phases is defined as $p_c = p_g - p_w$.

The stress relation is expressed by introducing the concept of the modified effective stress

$$\boldsymbol{\sigma}'' = \boldsymbol{\sigma} + \alpha \mathbf{m} p \tag{1}$$

in which $\boldsymbol{\sigma}$ is the total stress vector, $\boldsymbol{\sigma}''$ is the modified effective stress vector, $\mathbf{m}$ is the identity vector, p denotes the mean pore pressure applied by the porous fluids on the solid skeleton, which

is given by the averaging technique $p = S_w p_w + S_g p_g$, and α is the Biot constant. The constitutive equation of the solid phase in the continuum medium surrounding the crack is expressed by an incrementally linear modified effective stress-strain relationship

$$\mathrm{d}\boldsymbol{\sigma}'' = \mathbf{D}\,\mathrm{d}\boldsymbol{\varepsilon} \tag{2}$$

where **D** represents the tangential constitutive matrix of the continuum.

The non-linear behavior of the fracturing material in the cohesive zone is governed by a traction-separation law relating the cohesive tractions to the relative displacements

$$\mathbf{t}_d = \mathbf{t}_d(\llbracket \mathbf{u} \rrbracket) \tag{3}$$

where $\mathbf{t}_d$ is the cohesive traction transmitted across the fracture process zone and $\llbracket \mathbf{u} \rrbracket$ is defined as the relative displacement vector at the discontinuity. In quasi-brittle materials, as soon as the failure limit of the material is exceeded, the cohesive zone develops in which the material exhibits a softening behavior. Linearization of the cohesive relation (3) results in

$$\mathrm{d}\mathbf{t}_d = \mathbf{T}\,\mathrm{d}\llbracket \mathbf{u} \rrbracket \tag{4}$$

in which **T** represents the tangential modulus matrix of the discontinuity to be used in the iterative solution procedure, obtained from the relation $\mathbf{T} = \partial \mathbf{t}_d / \partial \llbracket \mathbf{u} \rrbracket$.

3 GOVERNING EQUATIONS

3.1 Strong form

In what follows, the equations specifying the problem are written in terms of the displacement of the solid phase, the pressure of the wetting phase and the capillary pressure. For a more detailed presentation of the governing equations see Ref. [9].

The linear momentum balance equation for the porous medium can be written as

$$\boldsymbol{\nabla} . \boldsymbol{\sigma} + \rho \mathbf{b} - \rho \ddot{\mathbf{u}} = \mathbf{0} \tag{5}$$

where $\ddot{\mathbf{u}}$ is the acceleration vector of the solid phase, **b** is the body force vector, ρ is the average density of the multiphase system defined as $\rho = (1-n)\rho_s + n\left(S_w \rho_w + S_g \rho_g\right)$, in which n stands for the porosity of the porous medium.

The continuity equations for the flow of wetting and non-wetting phase fluids through the deforming, isothermal porous medium can be written as

$$\begin{aligned} \frac{1}{Q_{ww}}\,\dot{p}_w + \frac{1}{Q_{wc}}\,\dot{p}_c + \alpha\,\boldsymbol{\nabla}.\dot{\mathbf{u}} + \boldsymbol{\nabla}.\dot{\mathbf{w}}_w + \boldsymbol{\nabla}.\dot{\mathbf{w}}_g = 0 \\ \frac{1}{Q_{cw}}\,\dot{p}_w + \frac{1}{Q_{cc}}\,\dot{p}_c + \alpha\,S_g\boldsymbol{\nabla}.\dot{\mathbf{u}} + \boldsymbol{\nabla}.\dot{\mathbf{w}}_g = 0 \end{aligned} \tag{6}$$

where $\dot{\mathbf{u}}$ is the solid velocity vector, and $\dot{\mathbf{w}}_w$ and $\dot{\mathbf{w}}_g$ are the Darcy velocity vectors of the two flowing fluids. The compressibility coefficients are defined as

$$\begin{aligned} \frac{1}{Q_{ww}} &= \frac{\alpha - n}{K_s} + \frac{nS_w}{K_w} + \frac{nS_g}{K_g} \\ \frac{1}{Q_{wc}} &= \frac{\alpha - n}{K_s}\left((1 - S_w) - p_c \frac{\partial S_w}{\partial p_c}\right) + \frac{nS_g}{K_g} \end{aligned} \tag{7}$$

$$\frac{1}{Q_{cw}} = \frac{(\alpha - n)S_g}{K_s} + \frac{nS_g}{K_g}$$

$$\frac{1}{Q_{cc}} = \frac{(\alpha - n)S_g}{K_s}\left((1 - S_w) - p_c\frac{\partial S_w}{\partial p_c}\right) - n\frac{\partial S_w}{\partial p_c} + \frac{nS_g}{K_g}$$

in which K_w and K_g are the bulk moduli of the porous fluids.

The Darcy relation for pore fluid flow can be written as

$$\dot{\mathbf{w}}_\alpha = \mathbf{k}_\alpha[-\boldsymbol{\nabla} p_\alpha + \rho_\alpha(\mathbf{b} - \ddot{\mathbf{u}})] \qquad \alpha = w, g \tag{8}$$

where $\mathbf{k}_w$ and $\mathbf{k}_g$ are the permeability matrices of the porous medium to the pore fluids, which are generally evaluated by the following expression

$$\mathbf{k}_\alpha = \mathbf{k}\frac{k_{r\alpha}}{\mu_\alpha} \qquad \alpha = w, g \tag{9}$$

in which $\mathbf{k}$ denotes the intrinsic permeability matrix of the porous medium, which is simply replaced by a scalar value k for the isotropic medium, $k_{r\alpha}$ is the relative permeability coefficient of the fluid, and μ_α denotes the dynamic viscosity of the fluid.

The permeability inside the fracture, i.e. the fully damaged zone and the micro-cracked zone, is strongly influenced by the change in the pore spaces of the solid skeleton as a result of cracking and micro-cracking processes. To this end, the pore fluid flow within the fracture is modeled by means of Darcy law with porosity dependent permeability, in which the dependence of the fracture permeability on the porosity is incorporated into the formulation via the coefficient k_{n_d}

$$\mathbf{k}_{\alpha d} = \mathbf{k}\frac{k_{n_d}k_{r\alpha}}{\mu_\alpha} \qquad \alpha = w, g \tag{10}$$

The following relation based on Ref. [10] is assigned to k_{n_d}

$$k_{n_d}(n_d) = 10^{\delta_{n_d}}, \qquad \delta_{n_d} = \frac{6(n_d - n)}{0.3 - 0.4n} \tag{11}$$

where n_d and n are the current and the initial porosity of the fracture material, respectively.

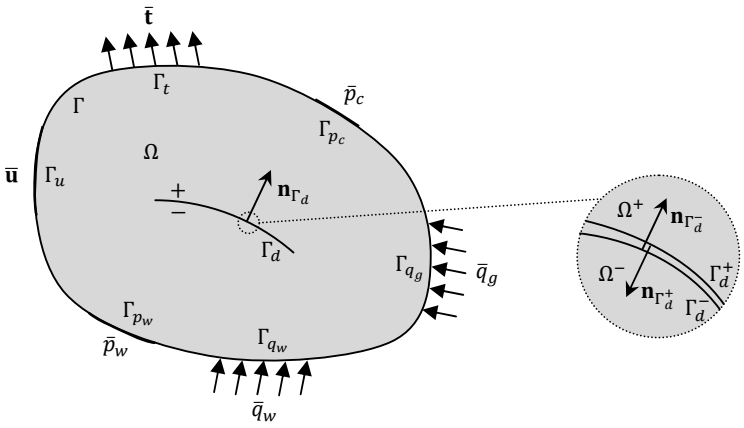

Figure 1: Boundary conditions of the body Ω involving the geomechanical discontinuity Γ_d

3.2 Weak form

To develop the equations, the two-dimensional domain Ω bounded by the boundary Γ is considered. As depicted in Fig. 1, the domain contains the geomechanical discontinuity Γ_d.

The weak form of the equilibrium equation for the multiphase system is given by

$$\int_{\Omega} \boldsymbol{\nabla}^{s}\boldsymbol{\eta} : \boldsymbol{\sigma}\, d\Omega + \int_{\Omega} \rho\boldsymbol{\eta}.\ddot{\mathbf{u}}\, d\Omega + \int_{\Gamma_d} [\![\boldsymbol{\eta}]\!].\left(\mathbf{t}_d - \alpha p\mathbf{n}_{\Gamma_d}\right) d\Gamma = \int_{\Gamma_t} \boldsymbol{\eta}.\bar{\mathbf{t}}\, d\Gamma + \int_{\Omega} \rho\boldsymbol{\eta}.\mathbf{b}\, d\Omega \tag{12}$$

which must hold for any kinematically admissible test function for the solid phase displacement $\boldsymbol{\eta}$, satisfying the homogenized essential boundary condition.

Incorporating Darcy law, the weak form of the continuity equation of flow for each of the fluid phases is given by

$$\begin{aligned}
&\int_{\Omega} \zeta_w \frac{1}{Q_{ww}}\dot{p}_w\, d\Omega + \int_{\Omega} \zeta_w \frac{1}{Q_{wc}}\dot{p}_c\, d\Omega + \int_{\Omega} \zeta_w \alpha\, \boldsymbol{\nabla}.\dot{\mathbf{u}}\, d\Omega + \int_{\Omega} \left(\mathrm{k}_w + \mathrm{k}_g\right)\boldsymbol{\nabla}\zeta_w\,.\boldsymbol{\nabla}p_w\, d\Omega \\
&\quad + \int_{\Omega} \mathrm{k}_g\, \boldsymbol{\nabla}\zeta_w\,.\boldsymbol{\nabla}p_c\, d\Omega + \int_{\Omega} \left(\mathrm{k}_w\rho_w + \mathrm{k}_g\rho_g\right)\boldsymbol{\nabla}\zeta_w\,.\ddot{\mathbf{u}}\, d\Omega - \int_{\Gamma_d} \zeta_w\left(q_{wd} + q_{gd}\right) d\Gamma \\
&\quad = \int_{\Omega} \left(\mathrm{k}_w\rho_w + \mathrm{k}_g\rho_g\right)\boldsymbol{\nabla}\zeta_w.\mathbf{b}\, d\Omega - \int_{\Gamma_{q_w}} \zeta_w\, \bar{q}_w\, d\Gamma - \int_{\Gamma_{q_g}\cap\,\Gamma_{q_w}} \zeta_w\, \bar{q}_g\, d\Gamma \\
&\quad - \int_{\Gamma_{p_c}\cap\,\Gamma_{q_w}} \zeta_w\, \dot{\mathbf{w}}_g.\mathbf{n}_{\Gamma}\, d\Gamma \\
&\int_{\Omega} \zeta_c \frac{1}{Q_{cw}}\dot{p}_w\, d\Omega + \int_{\Omega} \zeta_c \frac{1}{Q_{cc}}\dot{p}_c\, d\Omega + \int_{\Omega} \zeta_c \alpha\,(1 - S_w)\,\boldsymbol{\nabla}.\dot{\mathbf{u}}\, d\Omega + \int_{\Omega} \mathrm{k}_g\, \boldsymbol{\nabla}\zeta_c\,.\boldsymbol{\nabla}p_w\, d\Omega \\
&\quad + \int_{\Omega} \mathrm{k}_g\, \boldsymbol{\nabla}\zeta_c\,.\boldsymbol{\nabla}p_c\, d\Omega + \int_{\Omega} \mathrm{k}_g\rho_g\, \boldsymbol{\nabla}\zeta_c\,.\ddot{\mathbf{u}}\, d\Omega - \int_{\Gamma_d} \zeta_c\, q_{gd}\, d\Gamma \\
&\quad = \int_{\Omega} \mathrm{k}_g\rho_g\, \boldsymbol{\nabla}\zeta_c.\mathbf{b}\, d\Omega - \int_{\Gamma_{q_g}} \zeta_c\, \bar{q}_g\, d\Gamma
\end{aligned} \tag{13}$$

which must hold for any kinematically admissible test function for the wetting phase pressure ζ_w and the capillary pressure ζ_c, respectively, each disappearing on the boundary portion where the corresponding essential boundary condition is imposed. q_{wd} and q_{gd} are the leakage fluxes of the two pore fluids along the fracture toward the surrounding porous medium, which implies that there exists a discontinuity in the normal flow of the pore fluids across Γ_d. In order to arrive at a relation for the leakage flux of the pore fluids into the medium surrounding the discontinuity, the flow continuity equation for each flowing fluid inside the fracture is averaged over its cross section. Following this, the leakage terms appearing in the weak form of the wetting and non-wetting fluid flow continuity equations of the continuum medium are respectively obtained as

$$\begin{aligned}
q_{wd} + q_{gd} = &-2h\frac{1}{Q_{ww}}\,\dot{p}_w - 2h\frac{1}{Q_{wc}}\,\dot{p}_c - 2h\alpha\,\langle\frac{\partial\dot{u}_{x'}}{\partial x'}\rangle - \alpha\,[\![\dot{u}_{y'}]\!] \\
&-2h\,\frac{\partial}{\partial x'}\left(k_{wd}\left[-\frac{\partial p_w}{\partial x'} + \rho_w(b_{x'} - \langle\ddot{u}_{x'}\rangle)\right]\right)
\end{aligned} \tag{14}$$

$$-2h\ \frac{\partial}{\partial x'}\left(k_{gd}\left[-\frac{\partial p_w}{\partial x'}-\frac{\partial p_c}{\partial x'}+\rho_g(b_{x'}-\langle\ddot{u}_{x'}\rangle)\right]\right)$$

$$q_{gd}=-2h\frac{1}{Q_{cw}}\ \dot{p}_w-2h\frac{1}{Q_{cc}}\ \dot{p}_c-2h\alpha(1-S_w)\left\langle\frac{\partial \dot{u}_{x'}}{\partial x'}\right\rangle-\alpha(1-S_w)\left[\!\left[\dot{u}_{y'}\right]\!\right] \tag{15}$$
$$-2h\ \frac{\partial}{\partial x'}\left(k_{gd}\left[-\frac{\partial p_w}{\partial x'}-\frac{\partial p_c}{\partial x'}+\rho_g(b_{x'}-\langle\ddot{u}_{x'}\rangle)\right]\right)$$

in which the notation $[\![*]\!]=*^{+}-*^{-}$ represents the difference between the corresponding values at the two fracture faces and $\langle*\rangle=(*^{+}+*^{-})/2$ is specified as the average of the corresponding values at the discontinuity faces.

4 DISCRETIZATION OF THE GOVERNING EQUATIONS AND SOLUTION PROCEDURE FOR THE DISCRETIZED SYSTEM

In order to account for the displacement jump across the fracture, the displacement field should be discontinuous. In addition, to take into account each fluid flow jump normal to the fracture, it is required that the water pressure and also the capillary pressure field be continuous, while their corresponding gradient normal to the fracture be discontinuous.

Thus, the extended finite element approximation of the displacement field is written as

$$\mathbf{u}^h(\mathbf{x},t)=\sum_{I\in\mathcal{N}}N_{uI}(\mathbf{x})\ \mathbf{u}_I(t)+\sum_{I\in\mathcal{N}^{enr}}N_{uI}(\mathbf{x})\frac{1}{2}\left(H_{\Gamma_d}(\mathbf{x})-H_{\Gamma_d}(\mathbf{x}_I)\right)\ \tilde{\mathbf{u}}_I(t) \tag{16}$$

where $N_{uI}(\mathbf{x})$ is the standard finite element shape function of node I, $\mathcal{N}$ is the set of all nodes in the mesh, and $\mathcal{N}^{enr}$ is the set of enriched nodes defined as the set of nodes in the mesh whose support is bisected by the discontinuity. To ensure that the displacement jump is zero at the discontinuity tip, the nodes belonging to the element edge on which the discontinuity tip lies are not enriched. $\mathbf{u}_I(t)$ and $\tilde{\mathbf{u}}_I(\mathrm{t})$ are the standard and enriched degrees of freedom, respectively. The discontinuous function $H_{\Gamma_d}(\mathbf{x})$ is taken as the sign function centered on the line of the discontinuity Γ_d, i.e. $H_{\Gamma_d}(\mathbf{x})=\mathrm{sign}\big(\emptyset(\mathbf{x})\big)$, in which $\emptyset(\mathbf{x})$ is the level set function.

Symbolically, the enriched finite element approximation of the displacement field in Eq. (16) can be written in the following form

$$\mathbf{u}^h(\mathbf{x},t)=\mathbf{N}_u(\mathbf{x})\ \mathbf{U}(t)+\mathbf{N}_u^{enr}(\mathbf{x})\ \tilde{\mathbf{U}}(t) \tag{17}$$

in which $\mathbf{N}_u(\mathbf{x})$ is the matrix of the standard shape functions, and $\mathbf{N}_u^{enr}(\mathbf{x})$ is referred to as the matrix of the enriched shape functions. $\mathbf{U}(t)$ is the vector of the standard displacement degrees of freedom, and $\tilde{\mathbf{U}}(t)$ is the vector of the enriched displacement degrees of freedom.

The water pressure as well as the capillary pressure is approximated as

$$p_\alpha^h(\mathbf{x},t)=\sum_{I\in\mathcal{N}}N_{p_\alpha I}(\mathbf{x})\ p_{\alpha I}(t)+\sum_{I\in\mathcal{N}^{enr}}N_{p_\alpha I}(\mathbf{x})\left(D_{\Gamma_d}(\mathbf{x})-D_{\Gamma_d}(\mathbf{x}_I)\right)R(\mathbf{x})\ \tilde{p}_{\alpha I}(t) \tag{18}$$

where $N_{p_\alpha I}(\mathbf{x})$ are the standard finite element shape functions. Nodes in $\mathcal{N}^{enr}$ have their support bisected by the discontinuity. It is essential that the leakage flux vanish at the discontinuity tip. This is assured by requiring that the nodes on the element edge with which the discontinuity tip coincides not be enriched. $p_{\alpha I}(t)$ and $\tilde{p}_{\alpha I}(t)$ are the standard and enriched pressure degrees of freedom, respectively. $D_{\Gamma_d}(\mathbf{x})$ is the distance function, i.e. $D_{\Gamma_d}(\mathbf{x})=|\emptyset(\mathbf{x})|$. $R(\mathbf{x})$ is a weight

function with compact support given by

$$R(\mathbf{x}) = \sum_{I \in \mathcal{N}^{enr}} N_{p_\alpha I}(\mathbf{x}) \quad \alpha = w, c \tag{19}$$

It is noted that the multiplication with $R(\mathbf{x})$ causes the weighted enrichment function to vary continuously between the standard enrichment function and zero in the elements whose some nodes are in the enriched nodal set, reproducing the standard enrichment function in the elements whose all nodes are in the enriched nodal set. The enriched formulation in Eq. (18) has the form of the enrichment function in common with the modified formulation in [11,12], but the nodes chosen for enrichment conform with those of the standard one.

Likewise, the enriched finite element approximation of the water pressure and capillary pressure fields in Eq. (18) can be rewritten as

$$p_\alpha^h(\mathbf{x}, t) = \mathbf{N}_{p_\alpha}(\mathbf{x})\, \mathbf{P}_\alpha(t) + \mathbf{N}_{p_\alpha}^{enr}(\mathbf{x})\, \widetilde{\mathbf{P}}_\alpha(t) \qquad \alpha = w, c \tag{20}$$

Following Bubnov–Galerkin, the discretized form of the equations defining the multiphase problem is reached

$$\begin{aligned}
&\mathbf{M}_{uu}\ddot{\mathbf{U}} + \mathbf{M}_{u\tilde{u}}\ddot{\widetilde{\mathbf{U}}} + \int_\Omega \mathbf{B}^{\mathrm{T}}\boldsymbol{\sigma}'' \mathrm{d}\Omega - \mathbf{Q}_{uw}\mathbf{P}_w - \mathbf{Q}_{u\tilde{w}}\widetilde{\mathbf{P}}_w - \mathbf{Q}_{uc}\mathbf{P}_c - \mathbf{Q}_{u\tilde{c}}\widetilde{\mathbf{P}}_c = \mathbf{F}_u^{ext} \\
&\mathbf{M}_{u\tilde{u}}^{\mathrm{T}}\ddot{\mathbf{U}} + \mathbf{M}_{\tilde{u}\tilde{u}}\ddot{\widetilde{\mathbf{U}}} + \int_{\Omega^{enr}} (\mathbf{B}^{enr})^{\mathrm{T}}\boldsymbol{\sigma}'' \mathrm{d}\Omega - \mathbf{Q}_{\tilde{u}w}\mathbf{P}_w - \mathbf{Q}_{\tilde{u}\tilde{w}}\widetilde{\mathbf{P}}_w - \mathbf{Q}_{\tilde{u}c}\mathbf{P}_c - \mathbf{Q}_{\tilde{u}\tilde{c}}\widetilde{\mathbf{P}}_c \\
&\qquad + \mathbf{F}_{\tilde{u}}^{int} = \mathbf{F}_{\tilde{u}}^{ext} \\
&\mathbf{M}_{wu}\ddot{\mathbf{U}} + \mathbf{M}_{w\tilde{u}}\ddot{\widetilde{\mathbf{U}}} + \mathbf{Q}_{uw}^{\mathrm{T}}\dot{\mathbf{U}} + \mathbf{Q}_{\tilde{u}w}^{\mathrm{T}}\dot{\widetilde{\mathbf{U}}} + \mathbf{C}_{ww}\dot{\mathbf{P}}_w + \mathbf{C}_{w\tilde{w}}\dot{\widetilde{\mathbf{P}}}_w + \mathbf{C}_{wc}\dot{\mathbf{P}}_c + \mathbf{C}_{w\tilde{c}}\dot{\widetilde{\mathbf{P}}}_c \\
&\qquad + \mathbf{H}_{ww}\mathbf{P}_w + \mathbf{H}_{w\tilde{w}}\widetilde{\mathbf{P}}_w + \mathbf{H}_{wc}\mathbf{P}_c + \mathbf{H}_{w\tilde{c}}\widetilde{\mathbf{P}}_c - \mathbf{F}_w^{int} = \mathbf{F}_w^{ext} \\
&\mathbf{M}_{\tilde{w}u}\ddot{\mathbf{U}} + \mathbf{M}_{\tilde{w}\tilde{u}}\ddot{\widetilde{\mathbf{U}}} + \mathbf{Q}_{u\tilde{w}}^{\mathrm{T}}\dot{\mathbf{U}} + \mathbf{Q}_{\tilde{u}\tilde{w}}^{\mathrm{T}}\dot{\widetilde{\mathbf{U}}} + \mathbf{C}_{w\tilde{w}}^{\mathrm{T}}\dot{\mathbf{P}}_w + \mathbf{C}_{\tilde{w}\tilde{w}}\dot{\widetilde{\mathbf{P}}}_w + \mathbf{C}_{\tilde{w}c}\dot{\mathbf{P}}_c + \mathbf{C}_{\tilde{w}\tilde{c}}\dot{\widetilde{\mathbf{P}}}_c \\
&\qquad + \mathbf{H}_{w\tilde{w}}^{\mathrm{T}}\mathbf{P}_w + \mathbf{H}_{\tilde{w}\tilde{w}}\widetilde{\mathbf{P}}_w + \mathbf{H}_{\tilde{w}c}\mathbf{P}_c + \mathbf{H}_{\tilde{w}\tilde{c}}\widetilde{\mathbf{P}}_c - \mathbf{F}_{\tilde{w}}^{int} = \mathbf{F}_{\tilde{w}}^{ext} \\
&\mathbf{M}_{cu}\ddot{\mathbf{U}} + \mathbf{M}_{c\tilde{u}}\ddot{\widetilde{\mathbf{U}}} + \mathbf{Q}_{uc}^{\mathrm{T}}\dot{\mathbf{U}} + \mathbf{Q}_{\tilde{u}c}^{\mathrm{T}}\dot{\widetilde{\mathbf{U}}} + \mathbf{C}_{cw}\dot{\mathbf{P}}_w + \mathbf{C}_{c\tilde{w}}\dot{\widetilde{\mathbf{P}}}_w + \mathbf{C}_{cc}\dot{\mathbf{P}}_c + \mathbf{C}_{c\tilde{c}}\dot{\widetilde{\mathbf{P}}}_c \\
&\qquad + \mathbf{H}_{wc}^{\mathrm{T}}\mathbf{P}_w + \mathbf{H}_{\tilde{w}c}^{\mathrm{T}}\widetilde{\mathbf{P}}_w + \mathbf{H}_{cc}\mathbf{P}_c + \mathbf{H}_{c\tilde{c}}\widetilde{\mathbf{P}}_c - \mathbf{F}_c^{int} = \mathbf{F}_c^{ext} \\
&\mathbf{M}_{\tilde{c}u}\ddot{\mathbf{U}} + \mathbf{M}_{\tilde{c}\tilde{u}}\ddot{\widetilde{\mathbf{U}}} + \mathbf{Q}_{u\tilde{c}}^{\mathrm{T}}\dot{\mathbf{U}} + \mathbf{Q}_{\tilde{u}\tilde{c}}^{\mathrm{T}}\dot{\widetilde{\mathbf{U}}} + \mathbf{C}_{\tilde{c}w}\dot{\mathbf{P}}_w + \mathbf{C}_{\tilde{c}\tilde{w}}\dot{\widetilde{\mathbf{P}}}_w + \mathbf{C}_{c\tilde{c}}^{\mathrm{T}}\dot{\mathbf{P}}_c + \mathbf{C}_{\tilde{c}\tilde{c}}\dot{\widetilde{\mathbf{P}}}_c \\
&\qquad + \mathbf{H}_{w\tilde{c}}^{\mathrm{T}}\mathbf{P}_w + \mathbf{H}_{\tilde{w}\tilde{c}}^{\mathrm{T}}\widetilde{\mathbf{P}}_w + \mathbf{H}_{c\tilde{c}}^{\mathrm{T}}\mathbf{P}_c + \mathbf{H}_{\tilde{c}\tilde{c}}\widetilde{\mathbf{P}}_c - \mathbf{F}_{\tilde{c}}^{int} = \mathbf{F}_{\tilde{c}}^{ext}
\end{aligned} \tag{21}$$

The above equation system is then discretized in time domain following the line of the well-known Newmark scheme. To advance the solution in time, the link between the successive values of the unknown field variables at time t_{n+1} and the known field variables at time t_n is established by applying GN22 and GN11 to the displacement and pressure variables, respectively, as

$$\begin{aligned}
\ddot{\mathbf{U}}^{n+1} &= a_0\,(\mathbf{U}^{n+1} - \mathbf{U}^n) - a_2\,\dot{\mathbf{U}}^n - a_4\,\ddot{\mathbf{U}}^n \\
\dot{\mathbf{U}}^{n+1} &= a_1\,(\mathbf{U}^{n+1} - \mathbf{U}^n) - a_3\,\dot{\mathbf{U}}^n - a_5\,\ddot{\mathbf{U}}^n \\
\ddot{\widetilde{\mathbf{U}}}^{n+1} &= a_0\left(\widetilde{\mathbf{U}}^{n+1} - \widetilde{\mathbf{U}}^n\right) - a_2\,\dot{\widetilde{\mathbf{U}}}^n - a_4\,\ddot{\widetilde{\mathbf{U}}}^n \\
\dot{\widetilde{\mathbf{U}}}^{n+1} &= a_1\left(\widetilde{\mathbf{U}}^{n+1} - \widetilde{\mathbf{U}}^n\right) - a_3\,\dot{\widetilde{\mathbf{U}}}^n - a_5\,\ddot{\widetilde{\mathbf{U}}}^n \\
\dot{\mathbf{P}}_\alpha^{n+1} &= a_1'\,(\mathbf{P}_\alpha^{n+1} - \mathbf{P}_\alpha^n) - a_3'\,\dot{\mathbf{P}}_\alpha^n \qquad \alpha = w, c \\
\dot{\widetilde{\mathbf{P}}}_\alpha^{n+1} &= a_1'\left(\widetilde{\mathbf{P}}_\alpha^{n+1} - \widetilde{\mathbf{P}}_\alpha^n\right) - a_3'\,\dot{\widetilde{\mathbf{P}}}_\alpha^n \qquad \alpha = w, c
\end{aligned} \tag{22}$$

in which $a_0 = 1/\beta\Delta t^2$, $a_1 = \gamma/\beta\Delta t$, $a_2 = 1/\beta\Delta t$, $a_3 = \gamma/\beta - 1$, $a_4 = 1/2\beta - 1$, $a_5 = \Delta t(\gamma/2\beta - 1)$, $a_1' = 1/\theta\Delta t$ and $a_3' = 1/\theta - 1$. In these relations, $\Delta t = t_{n+1} - t_n$ is the time increment, and β, γ and θ are the Newmark parameters. To guarantee the unconditional stability of the time integration procedure, the Newmark parameters must be chosen such that $\gamma \geq 0.5$, $\beta \geq 0.25(0.5 + \gamma)^2$, and $\theta \geq 0.5$.

In order to resolve the system of fully coupled non-linear algebraic equations at each time step, the direct solution procedure is employed. In this numerical strategy, the discrete system of equations is solved at any specified time t_{n+1} applying the Newton–Raphson iterative algorithm to its residual form, $\boldsymbol{\Psi}^{n+1} = \mathbf{0}$. By expanding the residual equations with the first-order truncated Taylor series, the following linear approximation for the non-linear system to be solved is reached

$$\boldsymbol{\Psi}^{i+1,n+1} = \begin{Bmatrix} \boldsymbol{\Psi}_u^{i+1,n+1} \\ \boldsymbol{\Psi}_{\tilde{u}}^{i+1,n+1} \\ \boldsymbol{\Psi}_w^{i+1,n+1} \\ \boldsymbol{\Psi}_{\tilde{w}}^{i+1,n+1} \\ \boldsymbol{\Psi}_c^{i+1,n+1} \\ \boldsymbol{\Psi}_{\tilde{c}}^{i+1,n+1} \end{Bmatrix} = \begin{Bmatrix} \boldsymbol{\Psi}_u^{i,n+1} \\ \boldsymbol{\Psi}_{\tilde{u}}^{i,n+1} \\ \boldsymbol{\Psi}_w^{i,n+1} \\ \boldsymbol{\Psi}_{\tilde{w}}^{i,n+1} \\ \boldsymbol{\Psi}_c^{i,n+1} \\ \boldsymbol{\Psi}_{\tilde{c}}^{i,n+1} \end{Bmatrix} + \mathbf{J} \begin{Bmatrix} \mathrm{d}\mathbf{U}^{i+1,n+1} \\ \mathrm{d}\widetilde{\mathbf{U}}^{i+1,n+1} \\ \mathrm{d}\mathbf{P}_w^{i+1,n+1} \\ \mathrm{d}\widetilde{\mathbf{P}}_w^{i+1,n+1} \\ \mathrm{d}\mathbf{P}_c^{i+1,n+1} \\ \mathrm{d}\widetilde{\mathbf{P}}_c^{i+1,n+1} \end{Bmatrix} = \mathbf{0} \tag{23}$$

where $\mathbf{J}$ is the well-known Jacobian matrix, defined as $\partial\boldsymbol{\Psi}^{i,n+1}/\partial\mathbf{X}^{i,n+1}$ in which $\mathbf{X}$ represents the vector of nodal unknowns, $\mathbf{X} = [\mathbf{U}^{\mathrm{T}} \quad \widetilde{\mathbf{U}}^{\mathrm{T}} \quad \mathbf{P}_w^{\mathrm{T}} \quad \widetilde{\mathbf{P}}_w^{\mathrm{T}} \quad \mathbf{P}_c^{\mathrm{T}} \quad \widetilde{\mathbf{P}}_c^{\mathrm{T}}]^{\mathrm{T}}$. By finding the solution of the linearized system of equations (23), i.e. the increment of the standard and enriched nodal degrees of freedom, the corresponding nodal unknowns are subsequently attained through the incremental relation $\mathbf{X}^{i+1,n+1} = \mathbf{X}^{i,n+1} + \mathrm{d}\mathbf{X}^{i+1,n+1}$.

5 NUMERICAL SIMULATION RESULTS

The square plate with the edge crack of length $0.05\,m$ lying along its symmetry axis is simulated. The length sides of the plate is $0.25\,m$. The plate is loaded in tension by two uniform vertical velocities with magnitude $\bar{\dot{u}} = 2.35 \times 10^{-2}\ \mu m/s$ applied in opposite directions to the top and bottom edges of the plate. It is assumed that the plate has impervious boundaries to both fluids. Initially, the fully saturated condition is supposed. In the cohesive zone, the linear softening cohesive law is applied The material properties of the partially saturated porous medium are listed in Table 1. For fracture analysis, the cohesive fracture parameters of the material are set as follows: the cohesive strength $\sigma_c = 2.7$ MPa and the cohesive fracture energy $G_c = 95$ N/m.

The constitutive relations for the water saturation as well as the water and gas relative permeabilities are assumed on the basis of the van Genuchten-Mualem (VGM) model

$$\begin{aligned} S_w &= S_{rw} + (1 - S_{rw})\left[1 + \left(\frac{p_c}{p_{ref}}\right)^{1/(1-m)}\right]^{-m} \\ k_{rw} &= {S_e}^{1/2}\left[1 - \left(1 - {S_e}^{1/m}\right)^m\right]^2 \\ k_{rg} &= (1 - S_e)^{1/2}\left[1 - {S_e}^{1/m}\right]^{2m} \end{aligned} \tag{24}$$

in which the residual water saturation $S_{rw} = 0$, the empirical curve-fitting parameter $m = 0.4396$, the reference pressure $p_{ref} = 18.6$ MPa, and the effective water saturation S_e is defined as $S_e = (S_w - S_{rw})/(1 - S_{rw})$.

The numerical analysis of the plate is performed employing the three-phase model as well as the passive gas phase assumption. In these modelings, a comparison is made between the numerical results obtained considering the full coupling, i.e. the mechanical and the mass transfer coupling between the crack and the surrounding porous medium, and disregarding the mass transfer coupling. In the latter case, the interfacial flux vectors in the system of equations to be solved are omitted. Subsequently, the water pressure and capillary pressure fields need not be enriched any longer. Thus, the crack is not identified as a discontinuity in the fluid flow normal to the crack. That is, in the case without the mass transfer coupling term, no distinction is made between the flow of the pore fluids in the crack and in the porous medium surrounding the crack.

The numerical analysis continues until the crack tip gets to the right-hand side of the plate. The simulation results are presented for the time step before the crack propagates through the whole plate. Fig. 2 exhibits the contours of the water pressure for different simulations. As can be seen, incorporating the mass transfer coupling term into the simulation results in high negative water pressures concentrated in the vicinity of the crack, which implies that the pore water is drawn into the crack. These effects can also be distinguished in the contours of the gas pressure shown in Fig. 3, which result from the three-phase model. As observed in this figure, the negative pressures are greater in the case with full coupling than those without the mass transfer coupling. Moreover, it can be noticed that allowing for the interfacial flux along the crack leads to the considerable decrease of the gas pressure in the area surrounding the crack. This causes the pore gas to flow toward the crack. The gas pressure contours reveal that the values of the gas pressure, ignored in the model based on the assumption of the passive gas phase, can be as large as those of the water pressure. The impact of the incorporation of the mass transfer coupling on the results can further be evidenced by comparing the contours given in Figs. 4 and 5 representing the norm of the water pressure and gas pressure gradients, respectively. In accordance with what was observed before, pressure gradients with high values develop in the zone around the crack due to the mass transfer coupling. It also appears that the simulation in which all primary variables are enriched results in much higher values of the pressure gradient compared with those obtained without the water pressure and the capillary pressure enrichment. The results obtained with the passive gas phase assumption qualitatively correspond to those reported in Ref. [5].

Table 1: Material properties

Young's modulus	$E = 25.85$ GPa
Poisson's ratio	$\nu = 0.18$
Biot's constant	$\alpha = 1$
Initial porosity	$n = 0.2$
Solid phase density	$\rho_s = 2000$ kg/m^3
Water density	$\rho_w = 1000$ kg/m^3
Air density	$\rho_g = 1.2$ kg/m^3
Bulk modulus of solid phase	$K_s = 13.46$ GPa
Bulk modulus of water	$K_w = 0.2$ GPa
Bulk modulus of air	$K_g = 0.1 \times 10^{-3}$ GPa
Intrinsic permeability	$k = 2.78 \times 10^{-21}$ m^2
Dynamic viscosity of water	$\mu_w = 5 \times 10^{-4}$ Pa s
Dynamic viscosity of air	$\mu_g = 5 \times 10^{-6}$ Pa s
Atmospheric pressure	$p_{atm} = 0$ Pa

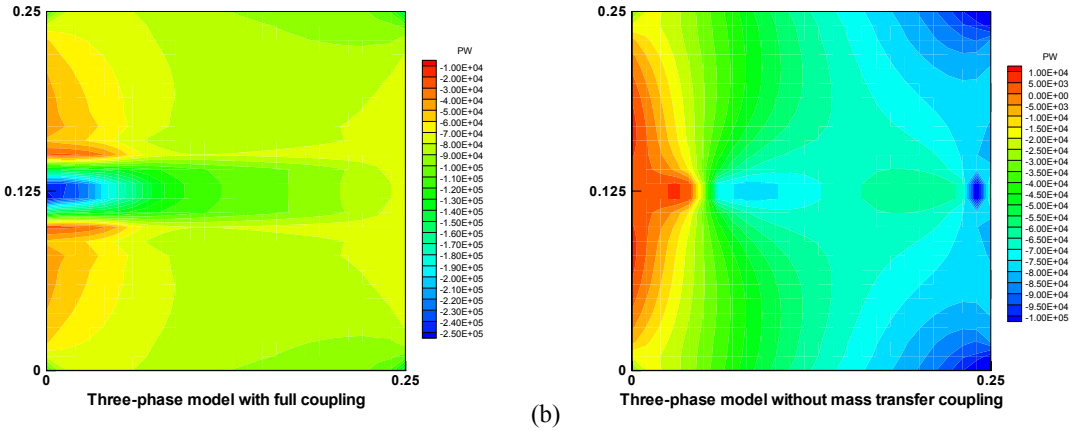

(a) (b)

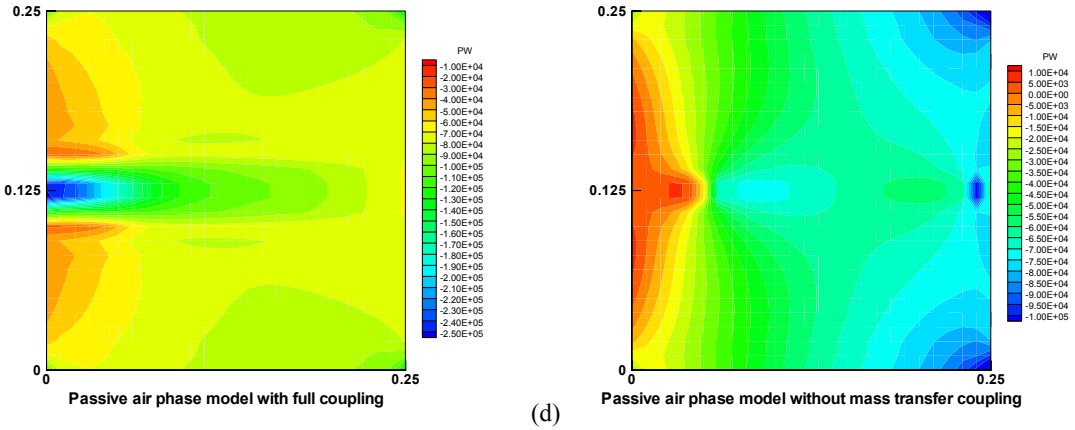

(c) (d)

Figure 2: Water pressure (Pa) contours: (a) three-phase model with full coupling, (b) three-phase model without mass transfer coupling, (c) passive air phase model with full coupling and (d) passive air phase model without mass transfer coupling

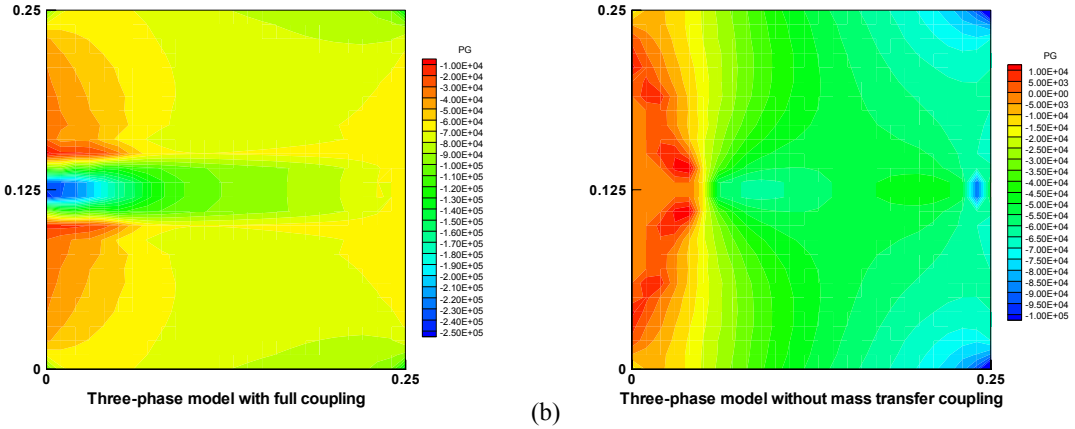

(a) (b)

Figure 3: Gas pressure (Pa) contours: (a) three-phase model with full coupling and (b) three-phase model without mass transfer coupling

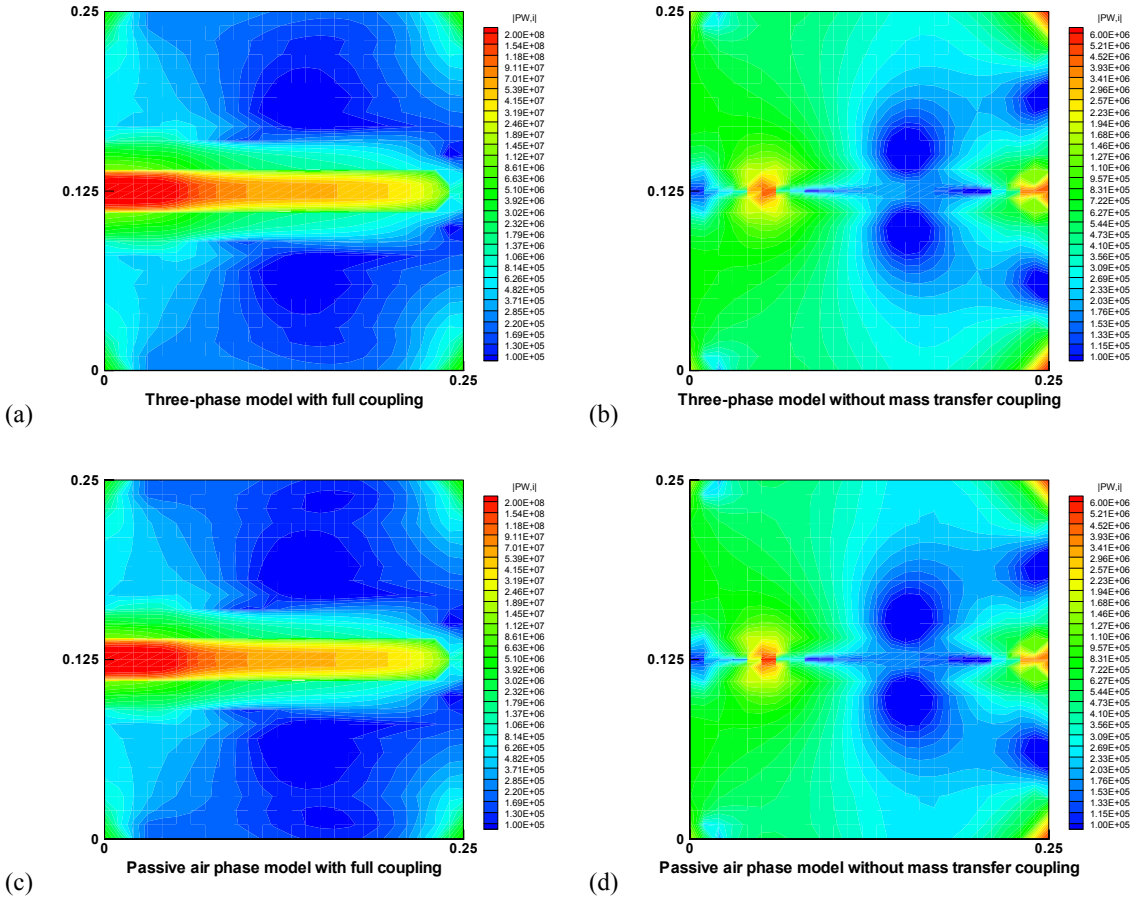

Figure 4: Norm of the water pressure gradient (Pa/m) contours (logarithmic scale): (a) three-phase model with full coupling, (b) three-phase model without mass transfer coupling, (c) passive air phase model with full coupling and (d) passive air phase model without mass transfer coupling

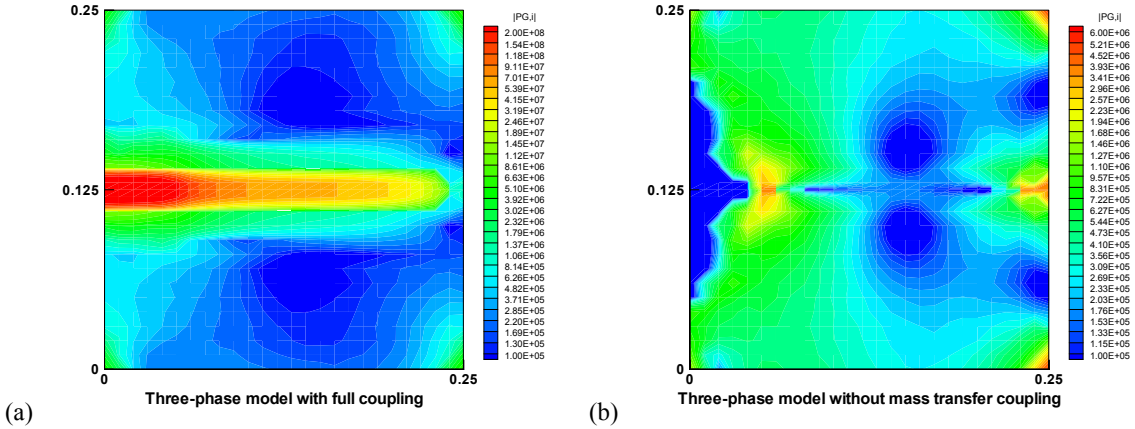

Figure 5: Norm of the gas pressure gradient (Pa/m) contours (logarithmic scale): (a) three-phase model with full coupling and (b) three-phase model without mass transfer coupling

6 CONCLUSIONS

In this paper, a numerical model was developed to simulate the flow of wetting and non-wetting pore fluids in progressively fracturing, partially saturated porous media in which the mechanical and the mass transfer coupling between the crack and the porous medium surrounding the crack were taken into account. For numerical simulation, the multiphase formulation was established based upon the linear momentum balance equation for the multiphase system and the flow continuity equation for each fluid phase. The cohesive crack concept was introduced, which gives the possibility to describe the non-linear behavior of the quasi-brittle material in the fracture process zone. In numerical modeling, the partition of unity property of finite element shape functions was exploited, which allows the local characteristic to be incorporated into the standard finite element approximation. The proposed method was successfully applied to the example involving a plate with a propagating cohesive crack, which puts in evidence the performance and applicability of the method. As illustrated in this example, the results are highly affected by inserting the discontinuity in the pressure normal derivative and thus considering the mass transfer coupling through the enrichment of the pressure field. In addition, it was verified that for a complete analysis of the problem the three-phase model is needed to be employed.

REFERENCES

[1] Boone, T.J. and Ingraffea, A.R. A numerical procedure for simulation of hydraulically-driven fracture propagation in poroelastic media. *Int. J. Numer. Anal. Meth. Geomech.* (1990) **14**:27-47.

[2] Schrefler, B.A., Secchi, S., Simoni, L. On adaptive refinement techniques in multi-field problems including cohesive fracture. *Comput. Methods Appl. Mech. Engrg.* (2006) **195**:444-461.

[3] Segura, J.M. and Carol, I. Coupled HM analysis using zero-thickness interface elements with double nodes. Part I: Theoretical model. *Int. J. Numer. Anal. Meth. Geomech*. (2008) **32**:2083-2101.

[4] Rethore, J., de Borst, R. and Abellan, M.A. A two-scale approach for fluid flow in fractured porous media. *Int. J. Numer. Meth. Engng*. (2007) **71**:780-800.

[5] Rethore, J., de Borst, R. and Abellan, M.A. A two-scale model for fluid flow in an unsaturated porous medium with cohesive cracks. *Comput. Mech*. (2008) **42**:227-238.

[6] Wells, G.N. and Sluys, L.J. A new method for modelling cohesive cracks using finite elements. *Int. J. Numer. Meth. Engng*. (2001) **50**:2667-2682.

[7] Moes, N., Belytschko, T. Extended finite element method for cohesive crack growth. *Engng. Fract. Mech.* (2002) **69**:813-833.

[8] Remmers, J.J.C., de Borst, R. and Needleman, A. The simulation of dynamic crack propagation using the cohesive segments method. J. *Mech. Phys. Solids* (2008) **56**:70-92.

[9] Khoei, A.R. and Mohammadnejad, T. Numerical modeling of multiphase fluid flow in deforming porous media: A comparison between two- and three-phase models for seismic analysis of earth and rockfill dams. *Comput. Geotech.* (2011) **38**:142-166.

[10] Meschke, G. and Grasberger, S. Numerical modeling of coupled hygromechanical degradation of cementitious materials. *J. Eng. Mech.* (2003) **129**:383-392.

[11] Fries, T-P. A corrected XFEM approximation without problems in blending elements. *Int. J. Numer. Meth. Engng*. (2008) **75**:503-532.

[12] Ventura, G., Gracie, R. and Belytschko, T. Fast integration and weight function blending in the extended finite element method. *Int. J. Numer. Meth. Engng*. (2009) **77**:1-29.